

Plant Pathol. J. 41(3): 253-265 (2025) https://doi.org/10.5423/PPJ.OA.12.2024.0188 eISSN 2093-9280

Research Article Open Access

# The Plant Pathology Journal

©The Korean Society of Plant Pathology

# Phytochemical Profiling and Antibacterial Activity of Cinnamon Bark Extract-Based Nanobactericides against Bacterial Panicle Blight in Rice

Qamar Mohammed Naji<sup>1,2</sup>, Dzarifah Mohamed Zulperi<sup>1,3</sup>\*, Khairulmazmi Ahmad<sup>1</sup>, and Erneeza Mohd Hata<sup>4</sup>

(Received on December 1, 2024; Revised on January 7, 2025; Accepted on January 16, 2025)

Bacterial panicle blight (BPB), caused by the aerobic Gram-negative bacterium Burkholderia glumae, poses a significant threat to global rice production. Cinnamon bark extract (CBE), rich in bioactive compounds such as eugenol and cinnamaldehyde, exhibits potent antioxidant and antimicrobial properties. To enhance the stability and efficacy of these volatile compounds, this study employed nanoencapsulation techniques. CBE-loaded nanoformulations were synthesized using the ionic coupling method between chitosan (CS) and trisodium phosphate (TPP) at varying TPP concentrations (0%, 0.5%, 1%, 2%, and 4%), resulting in CBE-CS nanoparticles. The nanoformulations were evaluated for antibacterial activity, chemical composition, and morphological characteristics. The antibacterial assays demonstrated inhibition zones ranging from 7.5 to 11.8 mm, with the 0.5% TPP formulation exhibiting the highest efficacy (minimum inhibitory concentration = 15.6 µmol/mL; minimum bactericidal concentration = 31.25 µmol/mL). Chemical analysis identified over 15 active compounds in CBE, with (Z)-3-phenylacrylaldehyde being the most abundant (34%). The nanoparticles had sizes ranging from 43.66 nm to 106.1 nm,

\*Corresponding author. E-mail) dzarifah@upm.edu.my

Handling Editor: Chang-Jin Park

Articles can be freely viewed online at www.ppjonline.org.

encapsulation efficiencies of 48.65–48.78%, and loading capacities of 25.65–33.9%. Scanning electron microscopy revealed spherical, homogenous nanoparticles, while Fourier transform infrared and X-ray diffraction confirmed the successful encapsulation of CBE within CS nanoparticles. Microscopic examination revealed significant membrane damage in *B. glumae* cells treated with CBE-loaded nanoparticles compared to untreated controls. These findings underscore the potential of CBE-loaded CS nanoencapsulation as an effective, ecofriendly solution for managing BPB. The study highlights the promise of nanoencapsulation techniques in enhancing the stability and bioactivity of natural antimicrobial agents, offering a sustainable alternative to traditional chemical controls in agriculture.

**Keywords**: bacterial panicle blight, *Burkholderia glumae*, cinnamon bark extract, nanoformulation, rice

Since the dawn of civilization, archaeological evidence suggests that rice (*Oryza sativa*) has been a fundamental food source for humans, with its cultivation dating back to 1,500–1,000 BC (Verma and Srivastav, 2020). Today, rice remains a staple food for approximately 40% of the global population, particularly in the least developed countries (Zhang et al., 2022). The optimal climatic conditions for rice cultivation, including high humidity and abundant water, are prevalent in many Asian countries, especially in tropical regions (Rashid et al., 2022). In Malaysia, rice is the third most important crop after rubber and oil palm, with the states of Kedah and Perlis being key centers of rice production. However, rice fields are highly susceptible to a

<sup>&</sup>lt;sup>1</sup>Department of Plant Protection, Faculty of Agriculture, Universiti Putra Malaysia, 43400 Serdang, Selangor, Malaysia <sup>2</sup>Directorate of the Planting of Holy Karbala, Iraqi Ministry of Agriculture, Karbala 56001, Iraq

<sup>&</sup>lt;sup>3</sup>Laboratory of Sustainable Resources Management, Institute of Tropical Forestry and Forest Products, Universiti Putra Malaysia, 43400 Serdang, Selangor, Malaysia

<sup>&</sup>lt;sup>4</sup>Institute of Plantation Studies, Faculty of Agriculture, Universiti Putra Malaysia, 43400 Serdang, Selangor, Malaysia

<sup>©</sup> This is an Open Access article distributed under the terms of the Creative Commons Attribution Non-Commercial License (http://creativecommons.org/licenses/by-nc/4.0) which permits unrestricted noncommercial use, distribution, and reproduction in any medium, provided the original work is properly cited.

variety of diseases caused by microbes, fungi, and bacteria, which can severely affect productivity. Over 70 different diseases have been identified as impacting rice fields, with five to six major bacterial diseases attacking various parts of the rice plant, including the seedlings, leaves, leaf sheath, grains, stem, and roots (Faizal Azizi and Lau, 2022). One of the most severe bacterial diseases affecting rice worldwide, including in Peninsular Malaysia, is bacterial panicle blight (BPB), caused by Burkholderia glumae (Ramachandran et al., 2021). This pathogen can cause up to a 75% yield loss and significantly reduce the quality of the affected plants, presenting a major challenge to rice cultivation. B. glumae thrives at optimal temperatures around 30°C, though it can survive in temperatures as high as 41°C. The bacteria infect seeds, enter plumules through stomata and wounds, and proliferate in the intercellular spaces of parenchyma during seed germination. This growth leads to the production of toxic substances like toxoflavin, which results in rice seedling rot (Rahman et al., 2024). Several strategies have been employed to manage BPB in rice cultivation (Chompa et al., 2022). Biological control methods, such as using harmless Burkholderia isolates, have been effective in reducing bacterial toxins and curbing rice grain rot. Cultural practices, including the use of pathogen-free seeds, also help limit bacterial transmission (Kumar et al., 2023). While chemical treatments like oxolinic acid have been used to control seedling and inflorescence rot (Han et al., 2021), the rise of resistant B. glumae strains and the negative residual effects of chemicals on soil and plants have decreased their use. Recently, natural plant extracts such as cinnamon bark have emerged as promising antibacterial agents for BPB control (Sharifi-Rad et al., 2021). Cinnamon, a widely used spice, is derived from the inner bark of trees belonging to the genus Cinnamomum (Farooq et al., 2023). Both the bark and leaves are used in cooking and in various natural medicinal applications. Cinnamon bark extract (CBE) is rich in bioactive compounds such as eugenol, cinnamaldehyde, cinnamic acid, and coumarin (Mini Raj et al., 2023). These components exhibit diverse pharmacological properties, including antifungal, antibacterial, anti-inflammatory, antioxidant, antidiabetic, nematocidal, insecticidal, and anticancer effects (Anuranj et al., 2022).

With significant advancements in plant disease control and the advent of nanotechnology, organic nanoparticles (ONPs) and nanostructures have emerged as a promising field for managing plant diseases (Koul et al., 2021). While many methods exist for synthesizing inorganic nanoparticles from metals like gold and silver or semiconductors such as Si, ZnO, Ge, and GaAs, fewer techniques are avail-

able for producing ONPs. Organic nanomaterials have gained attention due to their unique structural and optical properties, which differ from their bulk forms. One of the most promising polymers for delivering agrochemicals and micronutrients in nanoparticles (NPs) is chitosan (CS) (Mujtaba et al., 2020). CS is a natural amino polysaccharide derived from fungal cell walls, the exoskeletons of insects and crustaceans, and other natural sources. Commercially, CS is produced by partially de-N-acetylating chitin. It is considered more effective than chitin due to its higher content of chelating amino groups and greater chemical modifiability. As a cationic polyelectrolyte, CS exhibits unique properties, including its abundance, biocompatibility, biodegradability, and nontoxicity (Ul-Islam et al., 2024). Additionally, CS NPs offer great potential as nanocarriers, capable of encapsulating both hydrophilic and hydrophobic compounds (Pathak et al., 2023). In this study, the selection of CBE-CS and trisodium phosphate (TPP) as the primary components was driven by their complementary roles in achieving the study's objectives. CBE was chosen for its bioactive properties, particularly its volatile compounds with known antimicrobial activity. CS was selected due to its biocompatibility, biodegradability, and intrinsic antimicrobial properties, making it an ideal carrier for encapsulation. Together, CBE and CS form a synergistic system where CS provides structural support and controlled release, enhancing the stability and efficacy of the encapsulated compounds.

Tripolyphosphate was used as a cross-linking agent because of its ability to ionically interact with CS, enabling the formation of NPs with controlled size and charge. The concentration of TPP was found to be a critical factor in determining the hydrodynamic diameter of the NPs, influencing their stability, encapsulation efficiency, and bioavailability. This choice aligns with the study's objective to create a nanoencapsulation system that preserves the volatile compounds in CBE, protects them from oxidation, and ensures effective delivery to target pathogenic bacteria. This study contributes through the following points: (1) Nanoencapsulation for stability: The study develops a nanoencapsulation system using CBE, CS, and TPP to protect volatile compounds and enhance their antimicrobial effectiveness; (2) Enhanced bioactive delivery: Chitosan improves controlled release, increasing the bioavailability of CBE's bioactive compounds for targeting Burkholderia glumae, the cause of BPB; (3) Sustainable disease management: The study offers a sustainable alternative to chemical treatments by utilizing natural plant extracts and ONPs to manage BPB in rice fields.

### Materials and Methods

Raw materials. CS (molecular weight 200 kDa, with a deacetylation degree of ≥75%) was procured for the study. Cinnamon bark (*Cinnamonum cassia*) was sourced from local markets in Malaysia. The raw materials were carefully transported to the laboratories of the Department of Plant Protection, Faculty of Agriculture, Universiti Putra Malaysia UPM, where they were utilized for experimental procedures and subsequent evaluation of results.

Extraction of cinnamon bark extract. Cinnamon (Cinnamomum cassia) bark was obtained from market, wash, dry, and ground into a fine powder using a blender. The powdered cinnamon (20 g) was then macerated in 200 mL of methanol (70% v/v) in a tightly sealed container for 48 hours at room temperature with intermittent shaking. After maceration, the cinnamon-methanol mixture was filtered through Whatman filter paper (Grade 1). The filtrate was concentrated under reduced pressure using a rotary evaporator at 40°C to remove the methanol and obtain the concentrated cinnamon extract.

**Determination of the phytochemical compounds.** A gas chromatography/mass spectrometry (GC-MS) analysis was

performed to evaluate the volatile compounds and their abundances in CBE. This investigation using a (Shimadzu QP-2010 Ultra GC-MS system, Shimadzu Corporation, Kyoto, Japan) as described by Wang et al. (2020). The system features a gas chromatograph connected to a mass spectrometer and utilizes an SLB-5ms capillary column (30 m length  $\times$  0.25 mm ID  $\times$  0.25  $\mu$ m film thickness). The oven temperature program began at 50°C, then increased by 10°C per min to 250°C, and finally increased to 300°C. The analysis was conducted at 70 eV, with a scan interval of 0.1 s, recording fragments ranging from 40 to 700 Da.

Preparation of cinnamon bark extract-loaded CS submicron emulsions. A nanobacterial bactericide targeting *B. glumae* was prepared using CS loaded with CBE, following the method described by Maluin et al. (2019) with necessary modifications. The CBE was incorporated into CS NPs using ionic gelation technique. CS powder, sourced from Sigma Aldrich (low molecular weight, ≥ 75% deacetylation; St. Louis, MO, USA), was dispersed in a diluted acetic acid solution at a 1% (v/v) ratio and continuously stirred overnight at room temperature to form a 1% (w/v) CS solution. Subsequently, the CBE was mixed with Tween 80 (HLB 15.9) in a 1:1 (v/v) ratio, creating a CBE-Tween 80 mixture. This was stirred continuously for 1 h at room temperature until a homogeneous solution was

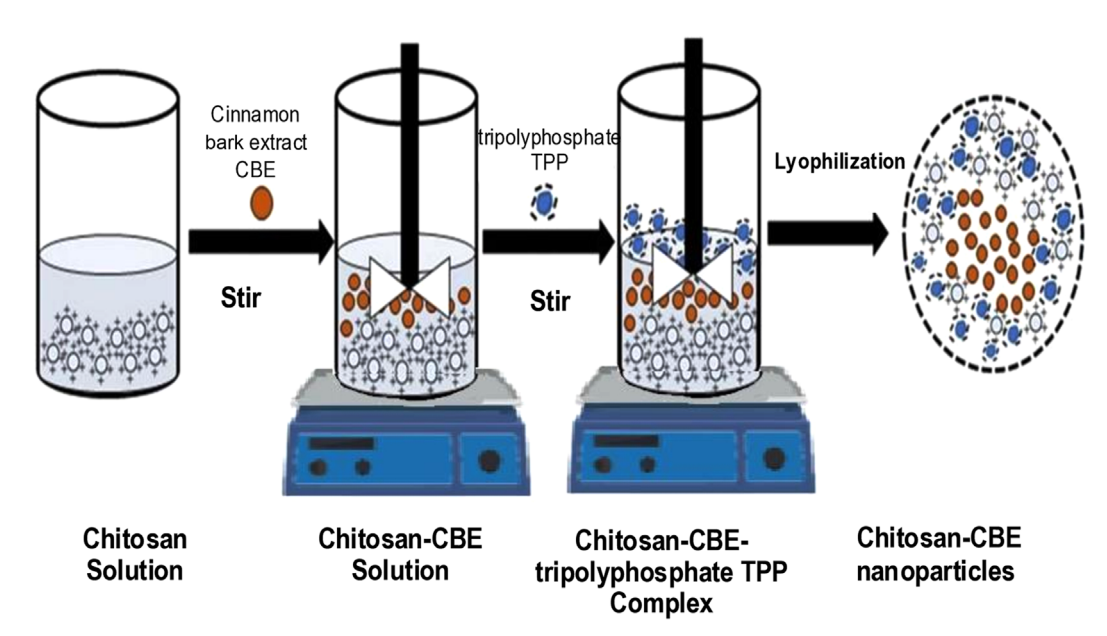


**Fig. 1.** Schematic representation of the preparation of chitosan nanocomposites loaded with cinnamon bark extract (CBE) using the ionic gelation method. Chitosan solution was combined with pre-prepared CBE in fixed proportions and mixed using magnetic stirring. Sodium triphosphate (TPP) at varying concentrations (0%, 0.5%, 1%, 2%, and 4%) was then added and thoroughly mixed. Sterile distilled water was incorporated to achieve a homogeneous mixture, resulting in four distinct concentrations of CBE-loaded nanocomposites.

achieved. To initiate cross-linking, a modified ionic gelation method was employed. A 5 mL portion of the 1% CS solution was combined with the CBE-Tween 80 mixture under continuous stirring until the mixture became viscous. TPP solutions at concentrations of 0%, 0.5%, 1%, 2%, and 4% (w/v) were then added to 15 mL of the CS mixture, stirred at 1,000 rpm for 15 min at room temperature. Finally, 5 mL of distilled water was added under magnetic stirring at room temperature and left for 24 h to complete the formulation. The resulting nanobactericidal formulation was designated CBE-CS. Fig. 1 illustrates the preparation process of CBE-CS.

## **Characterization of emulsions**

## Particle size, polydispersity index, and zeta potential.

The mean particle size (PS), polydispersity index (PDI), and zeta potential (ZP) of CBE-CS NPs were evaluated using a Zetasizer Nano ZS90 (Malvern Instruments Ltd., Malvern, UK) through dynamic light scattering at 25°C (Lunardi et al., 2021). ZP, determined from electrophoretic mobility using the Helmholtz-Smoluchowski equation under a 40 V/cm electric field, assessed NP stability by indicating potential variation between the dispersion medium and the stationary fluid layer (Ağardan, 2020). Morphology was examined via scanning electron microscopy after coating the samples with a thin carbon layer. Stability was tested by storing various formulations at room temperature. All measurements, conducted in triplicate (n = 3), utilized water's viscosity, refractive index, and absorption parameters provided by the Malvern software

**Transmission electron microscopy.** High-resolution transmission electron microscopy (TEM) was employed to investigate the morphology of CBE-CS NPs, with modifications to the method described by (Alghuthaymi et al., 2021). The samples were first diluted with distilled water and then deposited onto 200-mesh Formvar-coated copper grids for TEM imaging. The grids were subjected to low pressure and allowed to dry overnight at room temperature. The NPs were observed under TEM without any staining.

Fourier transform infrared spectroscopy. To analyze the active compounds in the CBE-CS nano-extract, Fourier transform infrared (FTIR) spectroscopy was employed. This technique was utilized to identify the various chemical bonds within the molecules by generating an IR absorption spectrum (Veerasingam et al., 2021). The materials analyzed included powdered CS and TPP, along with four liquid samples of the CBE-CS nano-extract and one sample of a simple CBE formulation for comparison.

Encapsulation efficiency and loading capacity. Encapsulation efficiency (EE) and loading capacity (LC) of CBE-CS nanobactericide formulations were evaluated using UV-Vis spectrophotometry with slight modifications to a standard protocol (Hoang et al., 2022). Freeze-dried nanobactericide (400 mg) was mixed with 5 mL of 1 M HCl, vortexed, and combined with 2 mL of ethanol, then incubated at 60°C for 12 h. After centrifugation at 6,000 rpm for 10 min at 25°C, the supernatant was analyzed with a UV-Vis spectrophotometer (200–400 nm). A calibration curve ( $R^2 = 0.9859$ ) was used to quantify CBE. Triplicate measurements ensured accuracy, and EE and LC were calculated using standard formulas (Hoang et al., 2022).

EE % 
$$\frac{\text{Weight of CBE in the nanoparticles}}{\text{The initial weight of CBE in the system}} \times 100$$
 (1)

In vitro release of nanobactericide formulation. The release analysis of the CBE-CS nanopesticide formulation was performed using a modified method from (Kaboudi et al., 2023). A 300  $\mu$ L sample of the formulation was dissolved in 30 mL of phosphate-buffered saline (PBS, pH 7.4) at room temperature. At specific intervals, 3 mL samples were collected for analysis, replacing the same volume with fresh PBS to maintain consistency. The released CBE concentration was measured using UV-Vis spectroscopy, and the total release was calculated using Eq. (3).

Release (%)= 
$$\sum_{t=0}^{\infty} \frac{M_t}{M_i} \times 100$$
 (3)

, where  $M_i$  represents the cumulative amount of CBE collected at time t, and  $M_i$  is the initial weight of CBE incorporated into the formulation. This formula provides the percentage of CBE released over time, reflecting the release kinetics and efficiency of the nanopesticide formulation.

# Evaluation of the antibacterial activity of CBE-CS.

The antibacterial efficacy of the nano-CBE-CS formulation against *B. glumae* was evaluated using disk diffusion assays. A *B. glumae* suspension ( $10^8$  colony forming unit [CFU]/mL) was prepared in sterile distilled water and spread evenly on Mueller-Hinton agar plates. Sterile Whatman filter paper discs (6 mm diameter) were impregnated with 20  $\mu$ L of formulations (CBE-CS 0, 0.5, 1, 2, and 4) in a laminar flow hood, with streptomycin ( $15 \mu$ g/mL) and distilled water serving as positive and negative controls, re-

spectively. The discs were placed on the inoculated plates, left at room temperature for 30 min for diffusion, and incubated at 37°C for 24 h. Inhibition zones were measured in millimeters, and bacterial inhibition percentages were calculated using Eq. (4). Each experiment was performed in triplicate and repeated twice (Chavez-Esquivel et al., 2021).

Inhibition effect (%) = 
$$\frac{\text{Extract inibition hold diameter (mm)}}{\text{Inhibition zone of positive control (mm)}} \times 100$$
 (4)

Minimum effective concentration and minimum bactericidal concentration (MBC) tests were performed by double dilution method on the CBE-CS nanobactericidal formulation at a concentration of 0.5% TPP due to the small diameter of the NPs and the high ZP value of this concentration.

Pathogenic bacteria growth curve analysis. To evaluate the bactericidal effects of the CBE-CS nanocide formulation, a growth curve analysis was conducted. In this study, a 96-well microplate was used to assess the bactericidal activity of the CBE-CS nanocide formulation. Each well was first filled with 150 μL of Mueller-Hinton broth, followed by the addition of 150 μL of the CBE-CS nanocide formulation at concentrations corresponding to 0.5 minimum inhibitory concentration (MIC), 1 MIC, and 2 MIC.

A control well received only 1% Tween 80. Subsequently, 50  $\mu$ L of *B. glumae* suspension (10<sup>7</sup> CFU/mL) was added to each well. The microplate was incubated at 37°C, and the optical density (OD) at 600 nm of the liquid culture was measured at regular intervals using a spectrophotometer to monitor bacterial growth (Cava-Roda et al., 2021).

### **Results and Discussion**

Determination of phytochemical constituents. The qualitative and quantitative analysis of CBE was conducted using GC-MS. Detailed on the various bioactive compounds found in CBE is presented in Table 1. The identification of constituents in CBE was performed by comparing their retention times and retention indexes with data from libraries such as FFNSC1.3.lib, NIST11.lib, and WILEY229. The gas chromatography analysis of CBE revealed the presence of 15 active substances. Among these compounds, (Z)-3-Phenylacrylaldehyde was found to be the most predominant, constituting 51.24% of the total composition. Following this, 2-propenoic acid, 3-(2-hydroxyphenyl) accounted for 13.24%, while cinnamaldehyde dimethyl acetal and hexadecanoic acid were present at concentrations of 11.23% and 5.48% respectively. Additionally, 2-propenal, 3-(2-methoxyphenyl) was identified at 3.99%, followed by eugenol (3.13%), oleic acid (2.23%), and eugenyl acetate (2.18%). Furthermore, 10(E),12(Z)-conjugated linoleic acid

**Table 1.** Phytochemical constituents in CBE identified by GC-MS, comparing Rt, RI, area %, molecular formula, MS, and height data with databases FFNSC1.3.lib, NIST11.lib, and WILEY229.lib

No.	Chemical component	Rt (min)	RI	Area (%)	Formula	MS	Height (%)
1	Cinnamaldehyde	21.165	1,218	0.58	C <sub>9</sub> H <sub>8</sub> O	373	1.08
2	(Z)-3-Phenylacrylaldehyde	23.707	1,189	51.24	$C_9H_8O$	295	37.12
3	Guaiacol	25.582	1,309	0.79	$C_9H_{10}O_2$	332	1.23
4	Eugenol	27.587	1,392	3.13	$C_{10}H_{12}O_2$	398	5.14
5	Coumarin	28.723	1,386	1.12	$C_9H_8O_2$	335	1.61
6	Cinnamaldehyde dimethyl acetal	29.477	1,287	11.23	$C_{11}H_{14}O_2$	361	16.77
7	2-Propenoic acid, 3-(2-hydroxyphenyl)	31.160	1,577	13.24	$C_9H_8O_3$	343	14.15
8	Muurolene	33.938	1,497	1.10	$C_{15}H_{24}$	404	1.60
9	Eugenyl acetate	34.917	1,521	2.18	$C_{12}H_{14}O_3$	388	3.21
10	2-Propenal, 3-(2-methoxyphenyl)-	35.063	1,378	2.99	$C_{10}H_{10}O_2$	363	4.31
11	1,3-Benzenediol, 4-propyl	37.942	1,434	1.95	$C_9H_{12}O_2$	367	2.20
12	Hexadecanoic acid	51.155	1,977	5.48	$C_{16}H_{32}O_2$	397	5.85
13	9-Octadecenoic acid (Z)-, methyl ester	55.625	2,085	0.68	$C_{19}H_{36}O_2$	383	1.08
14	10(E),12(Z)-Conjugated linoleic acid	56.660	2,183	2.06	$C_{18}H_{32}O_2$	371	2.06
15	Oleic acid	56.845	2,175	2.23	$C_{18}H_{34}O_2$	383	2.61

CBE, cinnamon bark extract; GC-MS, gas chromatography/mass spectrometry; Rt, retention times; RI, retention index; MS, mass spectrometry.

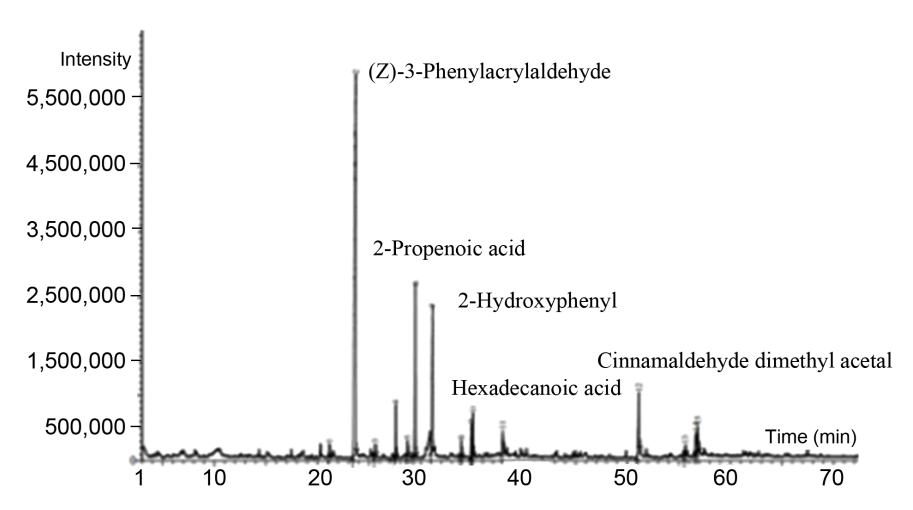


Fig. 2. Gas chromatography-mass spectrometry analysis of cinnamon bark extract: phytochemical profile and prominent peaks representing the concentration of major chemical compounds over time.

was detected at 2.06%. The analysis also revealed the presence of 4 aldehydes within the CBE. Apart from the compounds, the remaining constituents were found in smaller quantities, each comprising less than 2% of the specimen. Specifically, 1,3-benzenediol, 4-propyl was identified at 1.95%, followed by coumarin (1.12%), muurolene (1.10%), and guaiacol (0.79%). Additionally, 9-octadecenoic acid (Z)-, methyl ester and cinnamaldehyde were detected at concentrations of 0.68% and 0.58%, respectively. Fig. 2 illustrates the chemical analysis and characterization of CBE conducted using GC-MS, highlighting the identification of its key compounds.

**PS**, **PDI**, and **ZP**. The physical properties of nanomaterials such as PS, PDI, and ZP contribute to determining their behavior pattern within different biological environments. The size distribution was measured in a Zetasizer Pro (Malvern Instruments Ltd.) and the results obtained

represent the average value of three samples. While the ZP was measured in triplicate for the dispersed NPs of each NP suspension using a Zetasizer Pro with a DTS1070 zeta cell (Malvern Instruments Ltd.). From the results presented in Table 2, it is evident that the concentration of TPP plays a crucial role in determining the average hydrodynamic diameter of the particles in the CBE-CS. At 0% TPP, the particles exhibited a relatively large average size of 790.5 d.nm with a PDI index of 1, indicating significant polydispersity and potential instability in the formulation. As the TPP concentration was increased to 0.5%, there was a dramatic reduction in PS to 43.66 d.nm, accompanied by a more uniform distribution, as reflected by a lower PDI of 0.288. This initial decrease in size suggests that TPP may facilitate the formation of more stable, smaller NPs by promoting cross-linking within the extract. However, as the TPP concentration increased further, the average PS began to rise, with measurements of 51.72 d.nm (PDI 0.481) at 1% TPP,

Table 2. The impact of TPP concentration on the CBE-CS nanobactericide formulation's average PS, PDI, and ZP

Nano bactericide	Average size (d.nm)	PDI	ZP (mV)	Mobility (μm²/V·s)	Conductivity (mS/cm)
0% TPP	$435.68 \pm 22.14$ a	$1.00 \pm 0.00$ a	$7.79 \pm 0.04~a$	$-0.47 \pm 0.04 d$	$0.97 \pm 0.02 \; a$
0.5% TPP	$43.66 \pm 0.23$ a	$0.28 \pm 0.03~c$	$1.78 \pm 0.04 \; b$	$0.61 \pm 0.03~a$	$0.34 \pm 0.02\ c$
1% TPP	$51.72\pm0.04~a$	$0.57 \pm 0.02\;b$	$1.01\pm0.01\;b$	$-0.20\pm0.06~c$	$0.90 \pm 0.03~a$
2% TPP	$79.67 \pm 0.17$ a	$0.68 \pm 0.01\ b$	$-2.58\pm0.08\;c$	$0.13 \pm 0.03 \; b$	$0.53\pm0.07\;b$
4% TPP	$106.06 \pm 0.42$ a	$0.96\pm0.00\;a$	$-6.11 \pm 0.61 \ d$	$0.07 \pm 0.01 \; b$	$0.90 \pm 0.02 \; a$
Mean 1-30	1.08E + 04	0.661	0.396	0.03099	0.732
SD	1.96E + 04	0.325	4.81	0.3767	0.258

TPP, trisodium phosphate; CBE, cinnamon bark extract; CS, chitosan; PS, particle size; PDI, polydispersity index; ZP, zeta potential; SD, standard deviation.

79.82 d.nm (PDI 0.576) at 2% TPP, and 106.1 d.nm (PDI 0.96) at 4% TPP. This trend of increasing PS with higher TPP concentrations indicates a shift towards agglomeration, likely due to excessive cross-linking or the potential leakage of TPP onto the particle surfaces, which promotes sedimentation and aggregation. The increasing PDI values with higher TPP concentrations further support the notion of growing heterogeneity within the particle population (Das et al., 2020; Hasheminejad et al., 2019).

Consistent with earlier research, particularly studies by Huang et al. (2009) and Calvo et al. (1997), it was found that PDI values below 0.45 correspond to a narrow size distribution, like what was observed at 0.5% TPP in the current study. These previous studies demonstrated that the cross-linking of CS with TPP resulted in the formation of submicron particles with PDI values less than 1, which aligns with the findings of this investigation. In this study, the positive ZP values observed indicate a higher concentration of hydrogen ions (H+) relative to hydroxyl ions (OH-) around the particle surfaces. This phenomenon is typically attributed to the protonation of amino groups (NH<sub>3</sub><sup>+</sup>) present in CS (Prasad et al., 2022). The observed

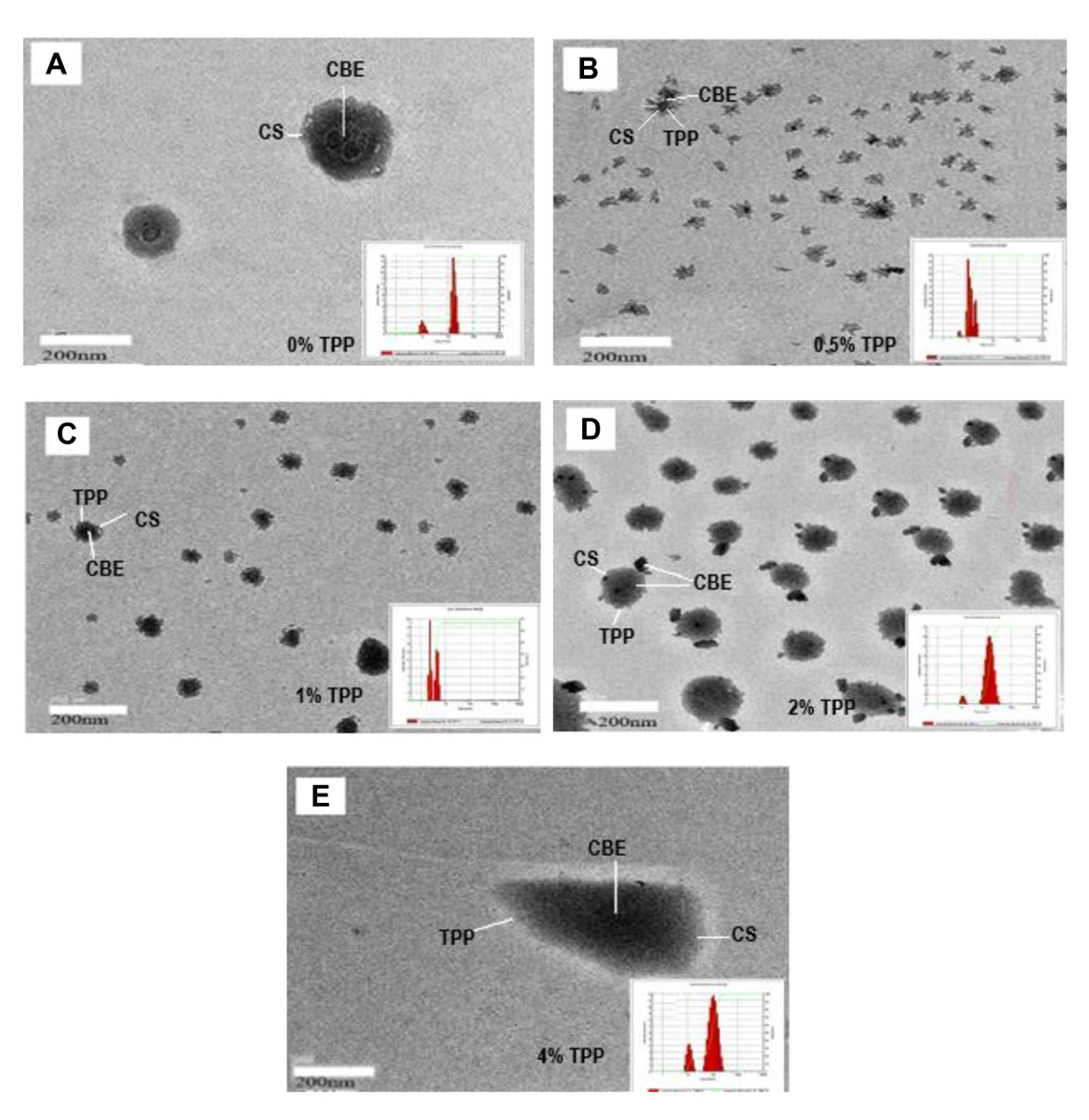


**Fig. 3.** Transmission electron microscopy (TEM) images of cinnamon bark extract (CBE) chitosan (CS) nanobactericidal formulations at varying trisodium phosphate (TPP) concentrations. TEM images display the formulations with TPP concentrations of 0% (A), 0.5% (B), 1% (C), 2% (D), and 4% (E) (scale bars = 200 nm). The darkest regions indicate the presence of CBE, moderately dark areas correspond to CS, and the lighter regions represent the TPP compound.

decrease in ZP values with increasing TPP concentrations suggests a reduction in positive peripheral charges. This is likely due to the interaction of TPP with the particle surface, which diminishes the number of protonated amino groups (NH<sub>3</sub><sup>+</sup>) on the CS particles (Fernández-Díaz et al., 2017). The study findings align with previous reports indicating that for an emulsion to remain physically stable, an electrical potential close to  $\pm 30$  mV is required. Notably, all concentrations of the nano-extract tested in the current experiment achieved this stability threshold. These results corroborate the findings of earlier studies, including those by (Deshi et al., 2024). In conclusion, the observed trend of increasing PS with higher TPP concentrations is not unique to this formulation but is a common phenomenon in similar studies involving CS-based NPs. This occurs due to the ionic interaction between the positively charged amino groups of CS and the negatively charged phosphate groups of TPP. As the TPP concentration increases, the degree of cross-linking and aggregation within the NPs also increases, resulting in larger particle sizes. Variations in morphology impact function: irregular, TPP-mediated particles enhance bacterial attachment and bioactive release, while overly smooth particles have less effective contact. TPP is crucial for optimizing morphology, ensuring stability, and enhancing antibacterial efficacy.

Evaluation of morphological change using TEM. The TEM images in Fig. 3A revealed that the nanocomposite was nearly circular when TPP was absent. In contrast, Fig. 3B–D demonstrated that the average size of the nanocomposite increased to 31 nm, 60 nm, and 73 nm for CBE-CS 0.5, CBE-CS 1, and CBE-CS 2, respectively, with a sharp and distinctly crystalline surface. The results also indicated that PS increased with rising TPP concentration, as observed in the TEM images. The spherical NPs exhibited lighter edges than their centers, suggesting TPP coating. Despite some particle clustering, the overall composition displayed a homogeneous distribution of the extract, with a distinctly crystalline NP surface.

Morphology and FTIR spectroscopy of emulsions. The results of FTIR spectroscopy analysis used to determine the chemical composition of the samples are shown in Fig. 4. The characteristic values of pure CS indicate the presence of many active chemical compounds, as the peak at 3,556/cm indicates the presence of O−H alcohol stretching, the peak at 3,329/cm indicates N−H stretching of the secondary amine, the peak at 2,24/cm indicates C≡N stretching, the peak at 1,519/cm indicates N−H bending, the peak at 1,068/cm indicates C−O stretching, while the peak at 732/

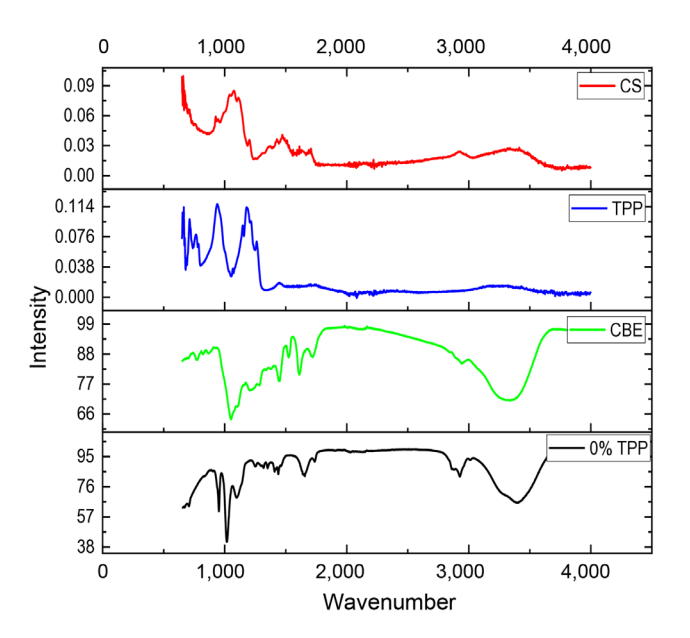


**Fig. 4.** Fourier transform infrared spectra of chitosan, tripolyphosphate (TPP), cinnamon bark extract (CBE), and CBE-chitosan nanoparticles (CBE-CS) at 0% TPP: identification of functional group vibrations and key chemical interactions.

cm indicates C=C bending. In the FTIR spectra of TPP, the peak at 1,127/cm corresponds to the O-P=O stretching vibration, while the peaks at 1,211/cm and 1,097/cm are associated with P=O and PO3 stretching vibrations, respectively, indicative of phosphorylated structures. Other significant peaks include 1,116, 1,087, and 1,028/cm (C-O, C-C, and C-H vibrations), all of which are crucial in characterizing the carbohydrate backbone. The infrared spectrum of cinnamon bark showed a sharp peak with high intensity at 1,662/cm, which indicates the stretching of the aldehyde carbonyl group C=O, which represents a high concentration of aldehyde in CB. Also, the presence of significant peaks at the range of 3,630 to 2,735/cm indicated the stretching of alcohol O-H, the peak at 1,134/cm indicated the stretching of C-O, and finally the peak at 759/cm indicated the bending of C=C. The cross-linking of the CS polymer with TPP and CBE in the different concentrations of nano-extract CBE-CS resulted in a significant change in the peak groups at the peak 3,329/cm related to amide (N-H stretching of secondary amine) and the peak at 3,379/ cm related to N-H stretching of primary amine. It is also evident that the peak shape became distinctly sharp due to the enhancement of hydrogen bonding, indicating the participation of TPP and amine groups in CS in the chemical reaction. While the presence of new absorption peaks at 2,870/cm indicates O-H stretching and at 1,624/cm indicates C=C stretching, while the high-intensity stretching

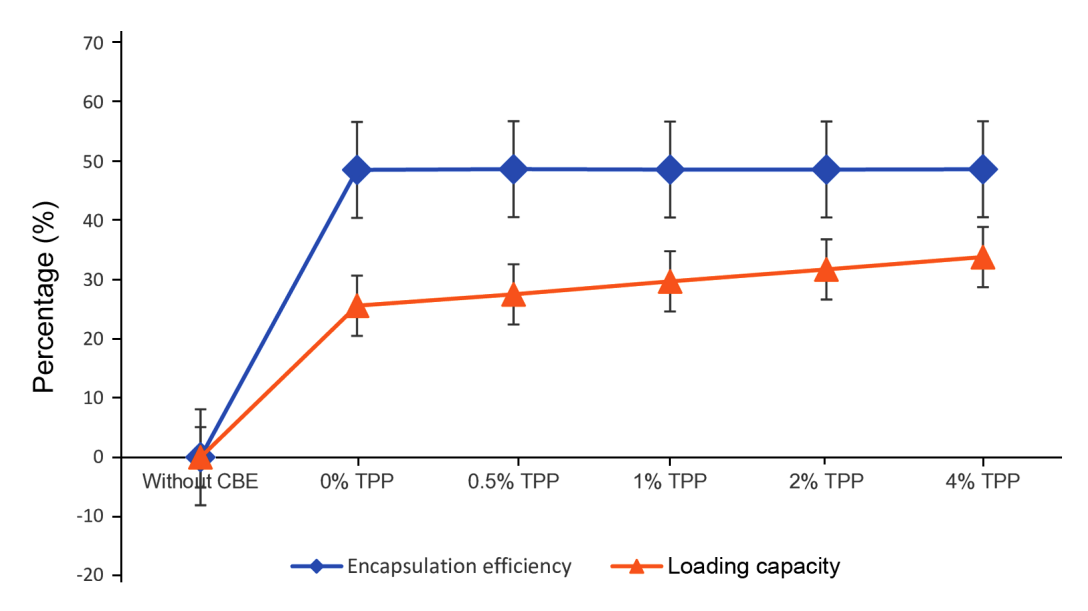


Fig. 5. Effect of cinnamon bark extract (CBE) loading at different trisodium phosphate (TPP) concentrations on encapsulation efficiency and loading capacity. Value indicates mean of four replicates.

band at 1,053/cm indicates C–O stretching. In the nano-extract CBE-CS at 0% of TPP, the distinct peaks at 1,662/cm indicated the extension of aldehyde carbonyl group by carbon = oxygen) and the peak at 1,134/cm indicated the extension of aldehyde carbonyl group. The results obtained in this study agree with the previous studies in references (Chaudhari et al., 2022; Das et al., 2020; Deepika et al., 2021; Prasad et al., 2022).

**EE** and LC. The EE and LC of CBE-CS nanocapsules were determined using UV-visible spectrophotometry at the maximum absorption wavelength of CBE-CS. The results, illustrated in Fig. 5, demonstrate the impact of varying TPP concentrations on the LC and EE of the nanocapsules. As the TPP concentration in the nanoemulsion increased, there was a notable positive effect on the LC of the nanocapsules. Specifically, the LC values rose from 25.65% to 33.9% as the TPP concentration increased from 0% to 4%. This trend indicates that higher TPP concentrations enhance the ability of the nanocapsules to incorporate CBE. However, if TPP is excessively increased, the NP structure might become too rigid and dense, which could reduce the available space for drug loading, thereby decreasing the LC. On the other hand, the EE remained relatively stable across all TPP concentrations, with values ranging between 48.65% and 48.78%. The consistent EE suggests that a saturation point may have been reached, beyond which further increases in TPP concentration do not significantly impact encapsulation. These findings are consistent with previous studies. For instance, Amiri et al.

(2021), Culas et al. (2023), and Deepika et al. (2021) also observed stable encapsulation efficiencies in similar formulations. Conversely, studies by Deepika et al. (2021) and Prasad et al. (2022) reported increases in both EE and LC with higher TPP concentrations.

*In vitro* release test. *In vitro* release kinetics test was performed where dried capsules were added in aqueousalcoholic medium at a volume ratio of 1:1. UV-visible spectroscopy at 286 nm wavelength was used to evaluate the concentration of CBE (Ramasamy et al., 2017). Readings were taken at times t = 0 (starting time), (t) 10, 20, 30, 60, 240, 1,440, and 2,880 min for triplicates. Fig. 6 shows the release of CB extract over time. As shown, after 1,440 min, the release rate of CB extract was 0.44 umol/mL. The curve is divided into two separate parts. The CBE concentration increases quickly in the first section, which corresponds to the test's initial hours. In enclosed systems, this behavior is frequently seen (Amiri et al., 2021). As the CBE contained in the capsule core slowly reaches the capsule surface, the second area of the curve shows a nearly constant CBE concentration (Sibaja et al., 2015; Shetta et al., 2019). Based on the concentration difference, these data show that the CBE release is connected to the concentration on the inside and external region of the capsule.

Assessment of antibacterial activity, MIC, and MBC. Inhibition zone formation, MIC, and MBC are critical measures of antimicrobial effectiveness. The *in vitro* evaluation

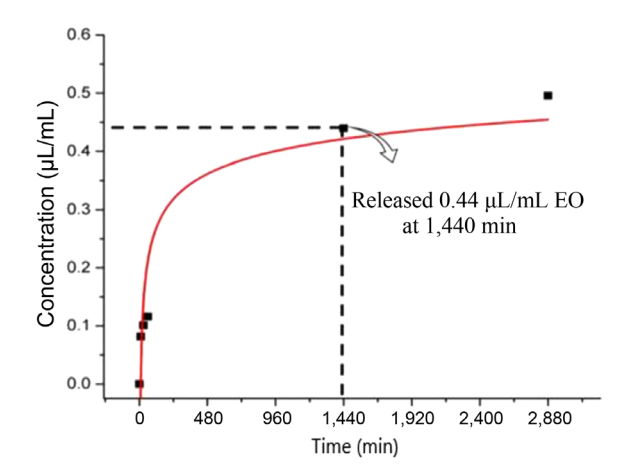


**Fig. 6.** Release kinetics of cinnamon bark extract over 48 h. The graph is divided into two phases: the first phase shows an increase in extract concentration over time until reaching the saturation point at 24 h, followed by the second phase, where the concentration stabilizes in the saturation region until 48 h.

of different CBE-CS nano-extract formulations against *B. glumae* demonstrated varying degrees of antibacterial efficacy, as measured by the diameter of inhibitory zones, the percentage of inhibited radial growth (PIRG), and the increment of activity of the test discs. The results, summarized in Table 3, reveal that all nanoformulations containing different concentrations of TPP were effective, albeit to varying extents.

The data indicates that the nano-extract with 0% TPP concentration exhibited the lowest inhibition zone, measuring 7.8 mm. As TPP concentrations increased, a corresponding significant increase in DIZ was observed, with values ranging from 11.5 to 11.8 mm for concentrations between 0.5% and 2% (P > 0.05). Notably, the nano-extract with 4% TPP concentration achieved a DIZ of 15.5 mm, while the positive control treated with streptomycin resulted in the highest DIZ at 24.6 mm, outperforming all other nanopesticide formulations. Furthermore, the PIRG index showed a positive correlation with increasing TPP concentrations, indicating enhanced antibacterial activity.

The most significant improvement in activity was observed at a TPP concentration of 0.5%, with a remarkable increment of 47.4% in effectiveness. When determining the MIC, the color change in the microtiter plate wells, which transitioned from colorless to bright red, indicated the presence of live bacteria and the varying impact of TPP concentrations on bacterial inhibition. The MIC value was determined to be 31.25  $\mu$ mol/mL, while the MBC value was 15.6  $\mu$ mol/mL. These findings underscore the potent antibacterial activity of the CBE-CS nano-extract against *B. glumae*, highlighting its potential as an effective antimicrobial agent.

Effect of nanostructures on bacterial growth curve. The growth curve asse was conducted to assess the bactericidal efficacy of CBE-CS 0.5% TPP nano-extract at varying concentrations of MIC (0.5, 1, and 2) against B. glumae. A bacteria-free control was used to establish a baseline, with its OD remaining steady after an initial increase during the first 18 h of incubation. The results of the growth curve are illustrated in Fig. 7. The nano-extract demonstrated a concentration-dependent effect on the growth rates of B. glumae throughout the 24-h period. All tested concentrations of MIC showed a reduction in bacterial growth rates within the first 4 h. For concentrations of 0.5 MIC and 1 MIC, a slight decrease in the growth rate was observed after the initial 4 h. In contrast, the nano-extract at 2 MIC exhibited a more pronounced impact, with a significant decrease in the growth curve observed after the first 4 h until 8 h. This result indicates that all MIC concentrations were highly effective, rapidly reducing the bacterial population and preventing further growth.

Conclusion. In this study, we developed a CBE-loaded nanoencapsulation aimed at controlling BPB caused by *Burkholderia glumae* in rice plants. The nanoencapsulation was formulated with varying concentrations of TPP (0%, 0.5%, 1%, 2%, and 4%) and characterized for its internal structure, morphology, and size using TEM. The results revealed that all NPs were within the nanometer scale,

**Table 3.** Disc diffusion method-based antimicrobial activities of CBE-CS nanobactericide formulation and the antibiotic streptomycin against *Burkholderia glumae* 

	CBE-CS formulation					AH O	Positive
	0% TPP	0.5% TPP	1% TPP	2% TPP	4% TPP	dH <sub>2</sub> O	control
Inhibition zone (mm)	$8.6\pm0.33~c$	$11.3 \pm 0.33 \text{ b}$	$11.5 \pm 0.28 b$	$11.6 \pm 0.76 \ b$	$11.3 \pm 0.33 \text{ b}$	$0.0 \pm 0.0 \; d$	$20.0 \pm 0.00 \; a$
PIRG (%)	31.7	46.7	47.1	47.9	46.0	-	-
Effectiveness increase (%)	-	47.4	0.8	1.72	-2.5	-	-

CBE, cinnamon bark extract; CS, chitosan; TPP, trisodium phosphate; PIRG, percentage of inhibited radial growth.

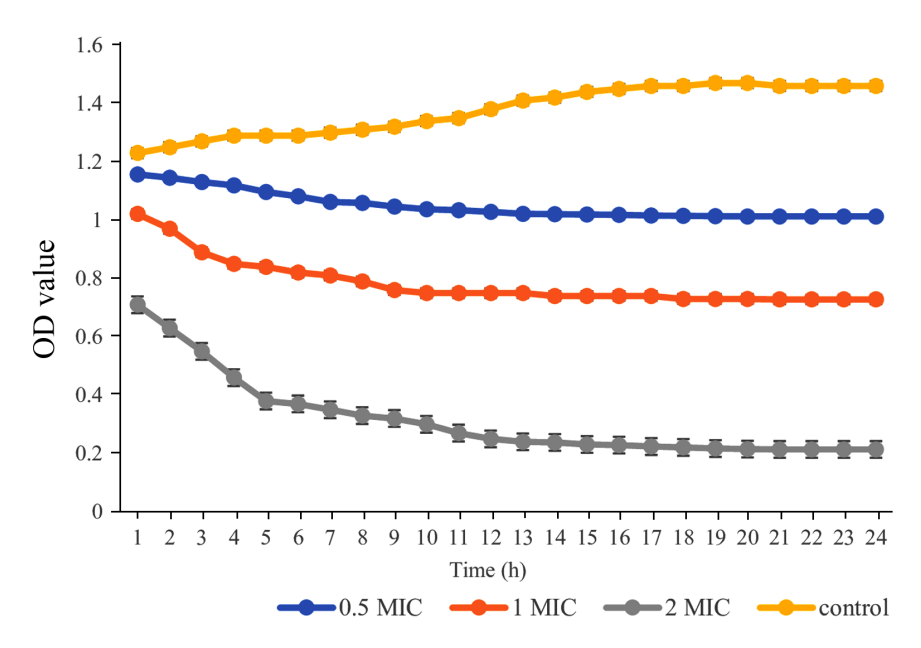


Fig. 7. Time killing analysis of the cinnamon bark extract-chitosan formulation against *Burkholderia glumae* at 0.5, 1, and 2 of minimum inhibitory concentration (MIC). The absorbance optical density (OD) at 600 nm was measured until the 24 h.

with the introduction of TPP significantly influencing their morphology. Specifically, TPP contributed to a more spherical shape, likely due to the increased rigidity from cross-linking between TPP and CS. PS analysis during dissolution in deionized water showed an inverse relationship between TPP concentration and NP size, with the smallest particles observed at 0.5% TPP. PDI analysis indicated a shift from monodisperse to polydisperse systems with higher TPP concentrations, suggesting decreased stability due to increased agglomeration. This instability may result from gel formation through inter- and intra-particle crosslinking. ZP measurements revealed that increasing TPP concentrations caused a shift from positive to negative surface charges, attributed to the negatively charged functional groups of cinnamon molecules coating the NPs. Higher ZP values indicate superior stability and functionality, while the observed negative ZPs may influence NP aggregation. FTIR analysis confirmed the successful encapsulation of CBE within the CS NPs, as evidenced by characteristic absorption bands and peaks associated with both CBE and CS functional groups. The release of bioactive substances from the NPs likely followed mechanisms such as disintegration, surface erosion, desorption, and diffusion. Initial rapid release within the first two hours, followed by a slower release, is crucial for effective bacterial control. The zone of inhibition tests confirmed the antibacterial efficacy of the CBE-CS nanobactericide against B. glumae, with a significant reduction in microbial count compared to the distilled

water-negative control, where no inhibition was observed. This suggests that the CBE-CS formulation offers promising potential for managing BPB in rice plants.

#### **Conflicts of Interest**

No potential conflict of interest relevant to this article was reported.

# Acknowledgments

We thank the financial support provided by University of Putra Malaysia UPM. We also thank the Iraqi Ministry of Agriculture represented by the Karbala Agriculture Directorate.

#### References

Ağardan, N. B. M. 2020. Studies on the formulation optimization and controlled ionic gelation of chitosan nanoparticles using TPP-HP-β-CD inclusion complex. *Istanbul J. Pharm.* 50:54-59.

Alghuthaymi, M. A., Diab, A. M., Elzahy, A. F., Mazrou, K. E., Tayel, A. A. and Moussa, S. H. 2021. Green biosynthesized selenium nanoparticles by cinnamon extract and their antimicrobial activity and application as edible coatings with nanochitosan. *J. Food Qual.* 2021:6670709.

Amiri, A., Ramezanian, A., Mortazavi, S. M. H., Hosseini, S. M. H. and Yahia, E. 2021. Shelf-life extension of pomegranate

arils using chitosan nanoparticles loaded with *Satureja hortensis* essential oil. *J. Sci. Food Agric.* 101:3778-3786.

- Anuranj, P. R., Harisankaran, P. S., Adithya Krishna, S., Parvathy, S., Prakash, G., Vishnu Savanth, V., Pran, M., Chopra, H., Emran, T. B., Dey, A., Dhama, K. and Chandran, D. 2022. Essential oils as valuable feed additive: a narrative review of the state of knowledge about their beneficial health applications and enhancement of production performances in poultry. J. Exp. Biol. Agric. Sci. 10:1290-1317.
- Calvo, P., Remuñán-López, C., Vila-Jato, J. L. and Alonso, M. J. 1997. Novel hydrophilic chitosan-polyethylene oxide nanoparticles as protein carriers. J. Appl. Polym. Sci. 63:125-132.
- Cava-Roda, R., Taboada-Rodríguez, A., López-Gómez, A., Martínez-Hernández, G. B. and Marín-Iniesta, F. 2021. Synergistic antimicrobial activities of combinations of vanillin and essential oils of cinnamon bark, cinnamon leaves, and cloves. *Foods* 10:1406.
- Chaudhari, A. K., Singh, V. K., Das, S., Deepika and Dubey, N. K. 2022. Fabrication, characterization, and bioactivity assessment of chitosan nanoemulsion containing allspice essential oil to mitigate *Aspergillus flavus* contamination and aflatoxin B<sub>1</sub> production in maize. *Food Chem.* 372:131221.
- Chavez-Esquivel, G., Cervantes-Cuevas, H., Ybieta-Olvera, L. F., Briones, M. T. C., Acosta, D. and Cabello, J. 2021. Antimicrobial activity of graphite oxide doped with silver against *Bacillus subtilis*, *Candida albicans*, *Escherichia coli*, and *Staphylococcus aureus* by agar well diffusion test: synthesis and characterization. *Mater. Sci. Eng. C Mater. Biol. Appl.* 123:111934.
- Chompa, S. S., Akter, A., Sadeq, A. B. M., Rahman, M. E., Rashid, H. O., Ibnat, N. and Hossain, M. B. 2022. An overview of major bacterial diseases of rice and management strategies for their control in Malaysia. *Glob. Sci. J.* 10:1074-1102
- Culas, M. S., Popovich, D. G. and Rashidinejad, A. 2023. Recent advances in encapsulation techniques for cinnamon bioactive compounds: a review on stability, effectiveness, and potential applications. *Food Biosci.* 57:103470.
- Das, S., Singh, V. K., Dwivedy, A. K., Chaudhari, A. K., Upadhyay, N., Singh, A., Deepika and Dubey, N. K. 2020. Fabrication, characterization and practical efficacy of *Myristica fragrans* essential oil nanoemulsion delivery system against postharvest biodeterioration. *Ecotoxicol. Environ. Saf.* 189:110000.
- Deepika, Singh, A., Chaudhari, A. K., Das, S. and Dubey, N. K. 2021. *Zingiber zerumbet* L. essential oil-based chitosan nanoemulsion as an efficient green preservative against fungi and aflatoxin B<sub>1</sub> contamination. *J. Food Sci.* 86:149-160.
- Deshi, V. V, Awati, M. G., Terdal, D., Patil, S. N., Ghandhe, A. R., Gudigennavar, A. S., Patalli, P., Lata, D., Singh, D. R. and Siddiqui, M. W. 2024. Cinnamon essential oil incorporated chitosan submicron emulsion as a sustainable alternative for extension of mango shelf life. Sustain. Chem. Pharm.

- 41:101736.
- Faizal Azizi, M. M. and Lau, H. Y. 2022. Advanced diagnostic approaches developed for the global menace of rice diseases: a review. Can. J. Plant Pathol. 44:627-651.
- Farooq, F., Hussain, Z., Hanief, M. I. and Fida, Z. 2023. Cinnamon (*Cinnamomum zeylanicum*): a brief review of the culinary spice with its potential therapeutic indications. *Eur. J. Biomed. Pharm. Sci.* 10:37-44.
- Fernández-Díaz, C., Coste, O. and Malta, E.-J. 2017. Polymer chitosan nanoparticles functionalized with *Ulva ohnoi* extracts boost *in vitro* ulvan immunostimulant effect in *Solea* senegalensis macrophages. *Algal Res.* 26:135-142.
- Han, V.-C., Yu, N. H., Park, A. R., Yoon, H., Son, Y. K., Lee, B.-H. and Kim, J.-C. 2021. First report of shot-hole on flowering cherry caused by *Burkholderia contaminans* and *Pseudomo*nas syringae pv. syringae. Plant Dis. 105:3795-3802.
- Hasheminejad, N., Khodaiyan, F. and Safari, M. 2019. Improving the antifungal activity of clove essential oil encapsulated by chitosan nanoparticles. *Food Chem.* 275:113-122.
- Hoang, N. H., Le Thanh, T., Sangpueak, R., Treekoon, J., Saengchan, C., Thepbandit, W., Papathoti, N. K., Kamkaew, A. and Buensanteai, N. 2022. Chitosan nanoparticles-based ionic gelation method: a promising candidate for plant disease management. *Polymers* 14:662.
- Huang, K.-S., Sheu, Y.-R. and Chao, I.-C. 2009. Preparation and properties of nanochitosan. *Poly. Plast. Technol. Eng.* 48:1239-1243.
- Kaboudi, Z., Peighambardoust, S. H., Nourbakhsh, H. and Soltanzadeh, M. 2023. Nanoencapsulation of Chavir (*Ferulago angulata*) essential oil in chitosan carrier: investigating physicochemical, morphological, thermal, antimicrobial and release profile of obtained nanoparticles. *Int. J. Biol. Macro-mol.* 237:123963.
- Koul, B., Poonia, A. K., Yadav, D. and Jin, J.-O. 2021. Microbemediated biosynthesis of nanoparticles: applications and future prospects. *Biomolecules* 11:886.
- Kumar, M., Kumar, A., Shukla, P., Mishra, A. K. and Kumar, A. 2023. Biology of rice bacterial brown stripe pathogen and integrated strategies for its management. *J. Exp. Agric. Int.* 45:1-8.
- Lunardi, C. N., Gomes, A. J., Rocha, F. S., De Tommaso, J. and Patience, G. S. 2021. Experimental methods in chemical engineering: zeta potential. *Can. J. Chem. Eng.* 99:627-639.
- Maluin, F. N., Hussein, M. Z., Yusof, N. A., Fakurazi, S., Idris, A. S., Hilmi, N. H. Z. and Jeffery Daim, L. D. 2019. A potent antifungal agent for basal stem rot disease treatment in oil palms based on chitosan-dazomet nanoparticles. *Int. J. Mol. Sci.* 20:2247.
- Mini Raj, N., Vikram, H. C., Muhammed Nissar, V. A. and Nybe, E. V. 2023. Cinnamon and Indian cinnamon (Indian Cassia). In: *Handbook of spices in India: 75 years of research and development*, eds. by P. N. Ravindran, K. Sivaraman, S. Devasahayam and K. N. Babu, pp. 2921-2991. Springer, Singapore.

- Mujtaba, M., Khawar, K. M., Camara, M. C., Carvalho, L. B., Fraceto, L. F., Morsi, R. E., Elsabee, M. Z., Kaya, M., Labidi, J., Ullah, H. and Wang, D. 2020. Chitosan-based delivery systems for plants: a brief overview of recent advances and future directions. *Int. J. Biol. Macromol.* 154:683-697.
- Pathak, R., Bhatt, S., Punetha, V. D. and Punetha, M. 2023. Chitosan nanoparticles and based composites as a biocompatible vehicle for drug delivery: a review. *Int. J. Biol. Macromol.* 253:127369.
- Prasad, J., Das, S., Maurya, A., Jain, S. K. and Dwivedy, A. K. 2022. Synthesis, characterization and *in situ* bioefficacy evaluation of *Cymbopogon nardus* essential oil impregnated chitosan nanoemulsion against fungal infestation and aflatoxin B<sub>1</sub> contamination in food system. *Int. J. Biol. Macromol.* 205:240-252.
- Rahman, A., Jahuddin, R., Bahar, A. K. F., Yani, A. and Patandjengi, B. 2024. Detection of the presence of bacteria causing grain rot disease (*Burkholderia glumae*) in some rice seed producers in South Sulawesi, Indonesia. *J. Trop. Plant Pests Dis.* 24:10-16.
- Ramachandran, K., Vijaya, S. I., Ahmad, F. N., Amzah, B. and Zakaria, L. 2021. Characterization and identification of *Bur-kholderia glumae* as the causal pathogen of bacterial panicle blight of rice (*Oryza sativa* L.) in Malaysian rice granaries. *J. Gen. Plant Pathol.* 87:164-169.
- Ramasamy, M., Lee, J.-H. and Lee, J. 2017. Direct one-pot synthesis of cinnamaldehyde immobilized on gold nanoparticles and their antibiofilm properties. *Colloids Surf. B Biointerfaces* 160:639-648.
- Rashid, M. R., Muhammad Zaidi, A. B., Noriha, M. A., Nur Sabrina, W., Hazalina, Z. and Noor Azlina, M. 2022. Preliminary screening of antagonistic rice-associated rhizobacteria on *Burkholderia glumae*. *Trans. Malaysian Soc. Plant Physiol*. 29:246-248.
- Sharifi-Rad, J., Dey, A., Koirala, N., Shaheen, S., El Omari, N., Salehi, B., Goloshvili, T., Cirone Silva, N. C., Bouyahya,

- A., Vitalini, S., Varoni, E. M., Martorell, M., Abdolshahi, A., Docea, A. O., Iriti, M., Calina, D., Les, F., López, V. and Caruntu, C. 2021. *Cinnamomum* species: bridging phytochemistry knowledge, pharmacological properties and toxicological safety for health benefits. *Front. Pharmacol.* 12:600139.
- Shetta, A., Kegere, J. and Mamdouh, W. 2019. Comparative study of encapsulated peppermint and green tea essential oils in chitosan nanoparticles: encapsulation, thermal stability, invitro release, antioxidant and antibacterial activities. Int. J. Biol. Macromol. 126:731-742.
- Sibaja, B., Culbertson, E., Marshall, P., Boy, R., Broughton, R. M., Solano, A. A., Esquivel, M., Parker, J., De La Fuente, L. and Auad, M. L. 2015. Preparation of alginate-chitosan fibers with potential biomedical applications. *Carbohydr. Polym.* 134:598-608.
- Ul-Islam, M., Alabbosh, K. F., Manan, S., Khan, S., Ahmad, F. and Ullah, M. W. 2024. Chitosan-based nanostructured biomaterials: synthesis, properties, and biomedical applications. Adv. Ind. Eng. Polym. Res. 7:79-99.
- Veerasingam, S., Ranjani, M., Venkatachalapathy, R., Bagaev, A., Mukhanov, V., Litvinyuk, D., Mugilarasan, M., Gurumoorthi, K., Guganathan, L., Aboobacker, V. M. and Vethamony, P. 2021. Contributions of Fourier transform infrared spectroscopy in microplastic pollution research: a review. *Crit. Rev. Environ. Sci. Technol.* 51:2681-2743.
- Verma, D. K. and Srivastav, P. P. 2020. Bioactive compounds of rice (*Oryza sativa* L.): review on paradigm and its potential benefit in human health. *Trends Food Sci. Technol.* 97:355-365.
- Wang, Y., Zhao, J., Xu, F., Wu, X., Hu, W., Chang, Y., Zhang, L., Chen, J. and Liu, C. 2020. GC-MS, GC-O and OAV analyses of key aroma compounds in Jiaozi Steamed Bread. *Grain Oil Sci. Technol.* 3:9-17.
- Zhang, J., Zhu, Y., Yu, L., Yang, M., Zou, X., Yin, C. and Lin, Y. 2022. Research advances in cadmium uptake, transport and resistance in rice (*Oryza sativa* L.). *Cells* 11:569.